J Porous Mater (2018) 25:171–178
DOI 10.1007/s10934-017-0430-1

Novel Al_2O_3–SiO_2 aerogel/porous zirconia composite with ultra-low thermal conductivity

Rubing Zhang[1] · Changshou Ye[1] · Baolin Wang[2]

Published online: 8 May 2017

Abstract Highly porous zirconia fibers networks with a quasi-layered microstructure were successfully fabricated using vacuum squeeze moulding. The effects of inorganic binder content on the microstructure, room-temperature thermal and mechanical properties of fibrous porous zirconia ceramics were systematically investigated. Al_2O_3–SiO_2 aerogel was impregnated into fibrous porous ceramics, and the microstructures, thermal and mechanical properties of Al_2O_3–SiO_2 aerogel/porous zirconia composites were also studied. Results show that the Al_2O_3–SiO_2 aerogel/porous zirconia composites exhibited higher compressive strength (i.e., 1.22 MPa in the z direction) and lower thermal conductivity [i.e., 0.049 W/(m/K)]. This method provides an efficient way to prepare high-temperature thermal insulation materials.

Keywords Fibrous ceramics · Aerogel · Thermal properties · Mechanical properties · Thermal insulation

1 Introduction

Zirconia (ZrO_2) is a very important ceramic material that is widely used in various areas such as electronics, catalysis and high-temperature structural engineering due to its superior acidic and basic catalytic characters, high thermal expansion coefficient, low thermal conductivity, high ionic conductivity and high thermal and chemical stability [1–4]. Highly porous ceramics can be engineered to combine several advantages inherent to their tailored porosity and architecture, such as fuel-cell electrodes, ceramic filters, catalyst supports and high-temperature light-weight insulation parts [4–7]. One effective way of further enhancing insulation performance of ZrO_2 ceramic is to increase the porosity and/or design the special pore structures. Recently, many processes were carried out to increase the porosity of porous ZrO_2 ceramics, such as adding fugitive substance, gel-casting and freeze casting [8–10]. Schlichting et al. [8] successfully fabricated porous zirconia ceramics using fugitive polymer method. Porous zirconia ceramics with high porosity of 52–76% and low thermal conductivity of 0.06–0.42 W/(m/K) were prepared by Hu et al. [9]. Hong et al. [10] fabricated porous zirconia ceramics with high porosity of 73.5–84.5 vol% and high compressive strength of 18–59 MPa by a camphene-based freeze-casting method. However, these porous ceramics exhibited low mechanical reliability due to using powder as a raw material.

In order to simultaneously obtain low thermal conductivity and high mechanical reliability, recently, fibrous porous ZrO_2 ceramics with a bird's nest structure were prepared using wet forming processes, such as gel-casting [11], freeze casting [12], and vacuum moulding [13]. Highly porous YSZ ceramics with low thermal conductivity [0.018–0.027 W/(m/K)] and relatively high compressive strength (0.34–0.66 MPa) were prepared through TBA-based gel-casting and pressureless sintering by using YSZ fibers as the raw material [11]. The bulk density and strength of fibrous porous ceramic fabricated by gel-casting were hard to control because the binders filled in the pores during the slurry gelatinization instead of stacking at the nodes of fibers [12]. Sun et al. fabricated porous fibrous zirconia ceramics with high porosity (72–89%), low thermal

✉ Rubing Zhang
rbzhang@bjtu.edu.cn; zrb86411680@126.com

[1] Department of Mechanics, School of Civil Engineering, Beijing Jiaotong University, Beijing 100044, China

[2] Institute for Infrastructure Engineering, Western Sydney University, Penrith, NSW 2751, Australia

conductivity [0.056–0.16 W/(m/K)], and relatively high compressive strength (0.6–13.3 MPa) [13]. In our previous studies [14, 15], novel quasi-layered structured mullite–zirconia fiber skeletons with higher strength have been prepared using vacuum squeeze moulding instead of vacuum moulding.

Aerogel is a kind of superinsulation material with mesoporous (2–50 nm) and ultra-high porosity (up to 90%). The nanoscale porous network structure significantly reduces the gaseous heat conduction and solid heat conduction of the material, which makes the thermal conductivity of aerogel material extremely low [16]. Therefore, aerogel is also seemed as one of promising insulation filler for impregnating into porous ceramics. In our previous work, a novel silica aerogel/porous Y_2SiO_5 composite was prepared by freeze casting and sol–gel impregnation [17]. Compared to porous Y_2SiO_5 ceramics, the compressive strength and thermal conductivity of the composites increased from 0.5–5.1 to 0.9–9.3 MPa and 0.079–0.286 to 0.069–0.260 W/(m/K), respectively. Recently, aerogels were also impregnated into fibrous porous mullite ceramics with bird's nest structure. Jiang et al. [18] prepared Al_2O_3–SiO_2 aerogel thermal insulation composites by impregnating SiC-coated mullite fibers with Al_2O_3–SiO_2 sol. The porous mullite fiber networks are filled by ZrO_2–SiO_2 aerogels to form aerogels/fibrous mullite ceramic composite [19]. The compressive strength (up to 1.05 MPa) is approximately twice of that of mullite fiber networks, and the thermal conductivity of the composite is much lower than the fiber networks. However, to the best of the authors' knowledge, the aerogels/fibrous porous zirconia ceramic composite has not been reported up to date.

In this work, novel porous zirconia fiber networks with a quasi-layered microstructure were fabricated by vacuum squeeze moulding, and the effect of inorganic binder on the microstructure and mechanical properties of fibrous porous zirconia ceramics were evaluated. In order to obtain ultra-high temperature insulation with higher compressive strength and lower thermal conductivity, Al_2O_3–SiO_2 aerogel was impregnated into fibrous porous zirconia ceramics. The microstructure, thermal and mechanical properties of Al_2O_3–SiO_2 aerogel/porous zirconia composites was also investigated. This paper may provide an insight on the synthesis of fibrous porous ceramics with ultra-low thermal conductivity and high strength for using as high-temperature thermal insulation material.

2 Experimental procedures

Commercially available polycrystalline zirconia fibers (8 mol% Y_2O_3–ZrO_2, Anhui Crystal New Materials Co. Ltd., China) with a diameter of 4–7 μm and a length of 300–500 μm were used as the raw material, which were added into the distilled water to form the mix slurries. Then 0.5 wt% polyacrylamide dispersant (Sigma-Aldrich Trading Co., Ltd., Shanghai, China), starch binder (5 wt% of the fibers, Sinopharm Chemical Reagent Co. Ltd., China), 5 wt% polyethyleneimine adsorbent (Sigma-Aldrich Trading Co., Ltd., China) and different inorganic binder contents were also added into the premix solution with continuous stirring. Then the slurry was squeezed to remove excess water and to form a soft felt under vacuum atmosphere. The detailed vacuum squeeze moulding process can be found in our previous work [14]. After drying in an oven at 80–100 °C for 24–28 h, the dried felt was sintered at 1400 °C for 1 h, with a heating rate of 3 °C/min. Finally, the sintered samples were machined to required shapes and sizes.

Aluminum chloride hexahydrate ($AlCl_3{\cdot}6H_2O$) and tetraethylorthosilicate [$Si(OC_2H_5)_4$, TEOS] were used as the aluminum and silicon precursors, respectively. Ethanol (EtOH) and propylene epoxide (PO) were used as the solvent and catalyst, respectively [18]. The sols were prepared according to the following steps: firstly, TEOS was dissolved and pre-hydrolyzed for 1.5 h, and then $AlCl_3{\cdot}6H_2O$ was dissolved in ethanol-aqueous solution to obtain Al_2O_3 sol. The Al_2O_3–SiO_2 sol was prepared by adding Al_2O_3 sol into the acidifying SiO_2 sol. The typical mole ratios were $AlCl_3{\cdot}6H_2O$:TEOS:EtOH:H_2O = 1:0.33:15:50. PO was added with vigorous stirring for 30 min. Then the Al_2O_3–SiO_2 sol was impregnated into the porous zirconia fiber networks under vacuum atmosphere. Wet gel was formed in the porous network of the porous zirconia ceramics by aging for 72 h at room temperature. The gel parts were subsequently soaked in a bath of absolute ethanol for 4 days to exchange the water. Finally, supercritical drying was performed (the critical point is T_c = 270 °C and P_c = 9.5 MPa for ethanol) to acquire non-cracked Al_2O_3–SiO_2 aerogel/porous zirconia composites.

The microstructure of the samples was observed by the scanning electron microscope (FEI Quanta 200, FEI Company, Hillsboro, USA). The bulk density was calculated based on the sample's weight and the corresponding volume. Porosity was calculated from the ratio of apparent density of porous sample to the theoretical density of dense ceramic. Each parameter was an average of the results of at least five samples. Nitrogen adsorption isotherms were measured with Quantachrome Autosorb-1. The pore size distribution was calculated by the Barrett–Joyner–Halenda (BJH) method. Thermal conductivity was measured by the guarded heat flow test method (DRE-III, Xiangtan Xiangyi Instrument Co., Ltd., Xiangtan, China). The compressive strength of the cylindrical samples with Φ 15 mm × 20 mm was measured by a testing machine (Zwick Z050, Zwick, Ulm, Germany) with a crosshead speed of 1.0 mm/min.

The samples were machined with the compressive surface perpendicular to the pressing direction. More than six samples of each measurement were selected to obtain the average value.

3 Results and discussion

Table 1 shows the effect of inorganic binder contents on porosities and densities of fibrous porous zirconia ceramics. When the B_4C content was increased from 0 to 4 wt% with a constant content of SiC (10 wt%), the density of the fibrous porous zirconia ceramics increased from 0.44 to 0.52 g/cm^3 and the porosity decreased from 92.8 to 91.5%. It indicates that the inorganic binder has an increased effect on the density of porous ceramics. The SEM images of the porous zirconia fiber networks with different inorganic binder contents were showed in Fig. 1. It can be seen in Fig. 1a that the zirconia fiber skeleton structure is anisotropic. Zirconia fibers were dispersed relatively uniformly in the *x*/*y* direction, and a quasi-layered structure was formed in the *z* direction. It can be attributed to the fact that an initial pressure was applied on the felt to preventing the rebinding and layering of the fiber skeleton during moulding. The result is similar to that reported by our previous work [13, 14]. Figure 1a–d showed the morphology of fibrous porous zirconia ceramics with different B_4C binder content. As the binder content was less than 2 wt%, no obvious grain growth was observed in the fibers, and only a thin borosilicate film was formed on the surface of fibers to bond the fibers at crossing points, which was obtained from B_4C and SiC under air atmosphere. However, when the B_4C binder content was increased to 2 wt%, the borosilicate glass phase increased. It was more easily gathered around the zirconia fiber junctions by the applied pressure, which can lead to an increase in the density of fibrous porous zirconia ceramics. Moreover, it might react with the zirconia fibers, which caused grain growth in the fibers (Fig. 1d). This can probably be due to the fact that the incensement of low melting points phase (B_2O_3) would lower the eutectic reacted temperature according to ZrO_2–B_2O_3–SiO_2 phase diagrams [20]. The morphology of fibrous porous zirconia ceramics with different SiC binder contents was shown in Fig. 1e, f. The borosilicate film was also formed on the surface of fibers and gathered around the zirconia fiber junctions. However, when the SiC content was increased from 10 to 20 wt% with a constant content of B_4C (1 wt%), the borosilicate glass phase increased. However, no obvious grain growth was observed in the ZrO_2 fibers (Fig. 1f). It indicated that the glass phase (SiO_2) does not react with ZrO_2 fibers which could not produce eutectic oxides at sintering temperature (1400 °C).

Fibrous porous ceramics are emerging as attractive engineering materials in aerospace applications, such as high-temperature thermal insulation tiles. The heat flow is predominantly in *z* direction. Hence, only the compressive strength and thermal conductivity of the samples in *z* direction are considered in this study. Table 1 shows the room-temperature compressive strength of the samples with different B_4C contents. As the B_4C content was increased from 0 to 1 wt%, the compressive strength of fibrous porous zirconia ceramics in the *z*-direction increased from 0.22 to 0.44 MPa, which is attributed to the decreased porosity of the sample. However, when the B_4C content further increased to 4 wt%, the compressive strength of the samples decreased to 0.31 MPa. The reason for lower compressive strength of the samples is the grain growth of the fibers with increasing B_4C content (as shown in Fig. 1), thus decreasing the strength of the zirconia fibers. The room-temperature thermal conductivity of the samples was also shown in Table 1. When the B_4C content was increased from 0 to 1 wt%, the thermal conductivity of fibrous porous zirconia ceramics decreased from 0.064 to 0.060 W/m/K. Then the thermal conductivity increased to 0.076 W/m/K as the B_4C content further increased to 4 wt%. When the B_4C content was 1 wt% or less, no obvious grain growth was observed in the fibers, and the porosities were almost the same, so the samples have the similar values of the thermal conductivity. However, when the B_4C content was increased from 1 to 4

Table 1 Porosity, density, compressive strength and thermal conductivity of fibrous porous zirconia ceramics with different inorganic binder contents

Inorganic binder (wt%)		Density (g/cm^3)	Porosity (%)	Strength (MPa)	Thermal conductivity (W/m/K)
SiC	B_4C				
10%	0%	0.44	92.8	0.22 ± 0.04	0.064 ± 0.002
	1%	0.46	92.5	0.44 ± 0.02	0.060 ± 0.001
	2%	0.50	91.8	0.34 ± 0.04	0.072 ± 0.003
	4%	0.52	91.5	0.31 ± 0.05	0.076 ± 0.004
10%	1%	0.46	92.5	0.44 ± 0.02	0.060 ± 0.001
15%		0.53	91.4	0.86 ± 0.04	0.066 ± 0.003
20%		0.55	91.0	0.91 ± 0.07	0.076 ± 0.002

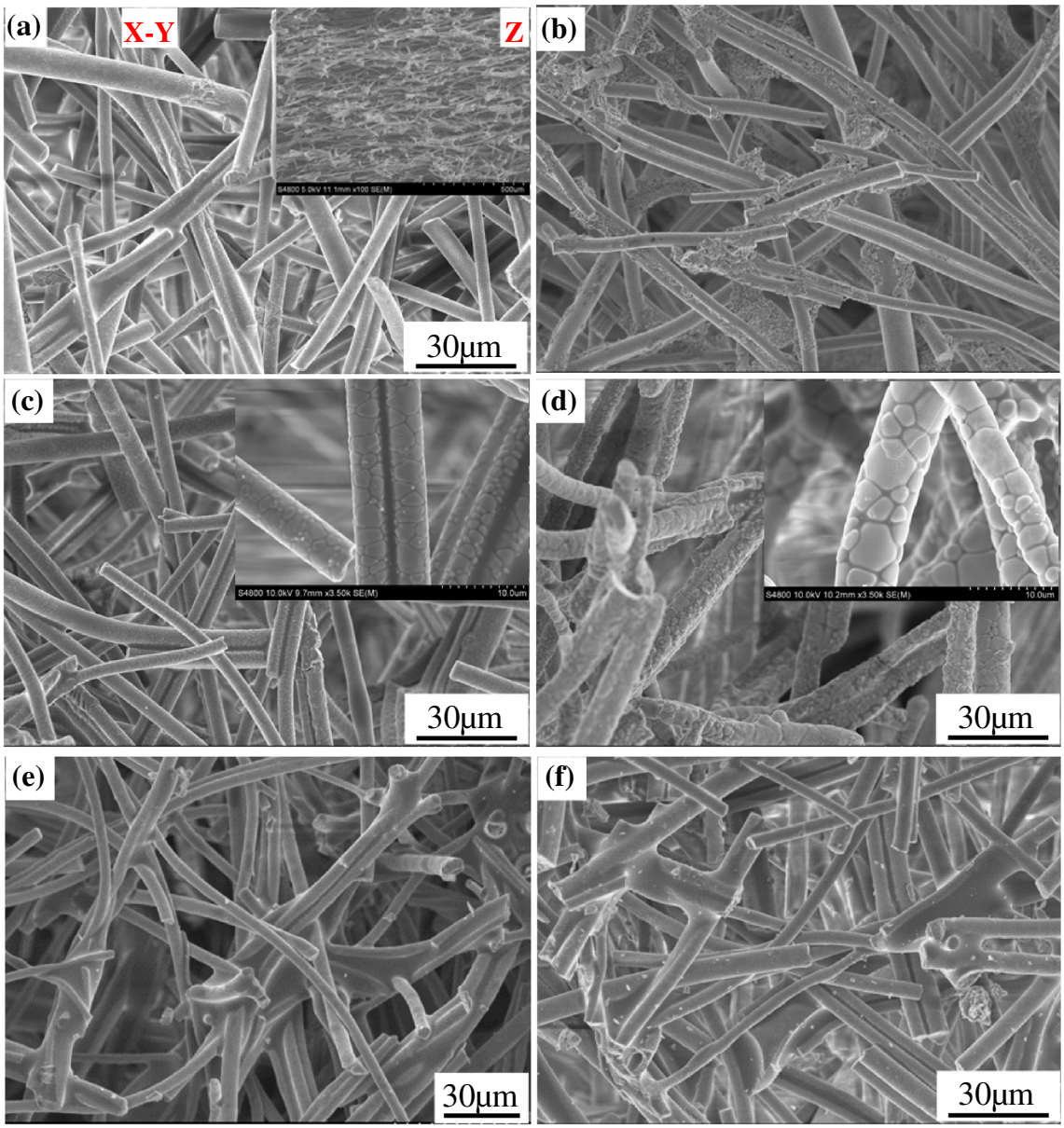

Fig. 1 SEM micrographs of fibrous porous zirconia ceramics with different inorganic binder contents: **a** 10% SiC + 1% B_4C; **b** 10% SiC; **c** 10% SiC + 2% B_4C; **d** 10% SiC + 4% B_4C; **e** 15% SiC + 1% B_4C; **f** 20% SiC + 1% B_4C

wt%, the increased thermal conductivity of the samples is affected by many factors. On one side, higher porosity in the porous ceramics reduces heat transfer by blocking the heat conduction pathways, and thus lowers the solid thermal conductivity. This is the main reason that the sample with higher B_4C content has lower porosity and higher thermal conductivity. On the other side, as the B_4C content increased, the degree of crystallization of fiber and binder became higher, which was the other reason for higher thermal conductivity [21]. Based on the above analysis, 1 wt% is the optimized B_4C content for obtaining low thermal conductivity and high mechanical strength, which has been confirmed by the SEM results (Fig. 1).

As seen in Table 1, when the SiC content was increased from 10 to 20 wt%, the density of the fibrous porous zirconia ceramics increased from 0.46 to 0.55 g/cm^3 and the porosity decreased from 92.5 to 91.0%; the compressive strength and thermal conductivity of fibrous porous zirconia ceramics in the *z*-direction increased from 0.40 to 0.91 MPa and 0.063 to 0.076 W/(m/K), respectively. As shown in Fig. 1, the borosilicate glass phase increased with increasing SiC content, with the result that the sample with higher SiC content has higher compressive strength and

thermal conductivity. The main reasons are the following two aspects: (1) the borosilicate glass phase formed on the surface of fibers increased the density of fibrous porous zirconia ceramics; (2) the increased borosilicate glass phase gathered around the zirconia fiber junctions, which enhanced the bonding strength between fibers and provided higher solid-phase heat conduction in these samples. These demonstrate that the zirconia fiber networks with higher SiC content are capable of increasing the thermal conductivity and strength of the porous ceramics.

Figure 2a, b exhibits the appearance of the obtained Al_2O_3–SiO_2 wet gels and aerogel. The initial Al_2O_3–SiO_2 wet gel is translucent (Fig. 2a). After aging for 3 days, the obtained Al_2O_3–SiO_2 aerogel shrinks by about 18% and becomes white and opaque with the density of about 0.14 g/cm^3 (Fig. 2b); moreover, no cracking occurs after supercritical drying. These shrinkages are similar to those of alumina aerogels prepared from $Al(NO_3)_3{\cdot}9H_2O$ [22]. The microstructures of fibrous porous zirconia ceramics before and after the impregnation of Al_2O_3–SiO_2 aerogel have been observed by SEM, as shown in Fig. 2c, d. It can be seen that the porous zirconia fiber networks were almost absolutely filled with Al_2O_3–SiO_2 aerogel (Fig. 2c), which indicated that Al_2O_3–SiO_2 aerogels can be easily impregnated into fibrous porous zirconia ceramics to form aerogels/fibrous ceramic composites. As shown in Fig. 2d, the Al_2O_3–SiO_2 aerogels formed in the composites still exhibits randomly interconnected 3-D porous networks made up of nanometer-sized spheroidal particles and nanopores. These observations show that the impregnation of Al_2O_3–SiO_2 aerogel is favourable for maintaining the three-dimensional mesoporous structure, which would further improve the thermal insulation performance.

Figure 3a shows the N_2 adsorption–desorption isotherms of unheated and heat-treated Al_2O_3–SiO_2 aerogel/porous zirconia composites. The unheated and 1000 °C treated composites showed similar isotherms, which present typical type IV curves [23]. The adsorption isotherms were almost unmodified in the small relative pressure region ($P/P_0 < 0.7$), whereas a noticeable enhancement at $P/P_0 > 0.9$. It implies that Al_2O_3–SiO_2 aerogel/porous zirconia composite is a micro–macroporous material, which is consistent with the porous structure observed in Fig. 2. Furthermore, relatively high specific volumes adsorbed at low P/P_0 values indicate the presence of a large amount of micropores [24]. The corresponding pore size distributions of unheated and heat-treated composites are shown in Fig. 3b, which show a pronounced peak in the mesopore

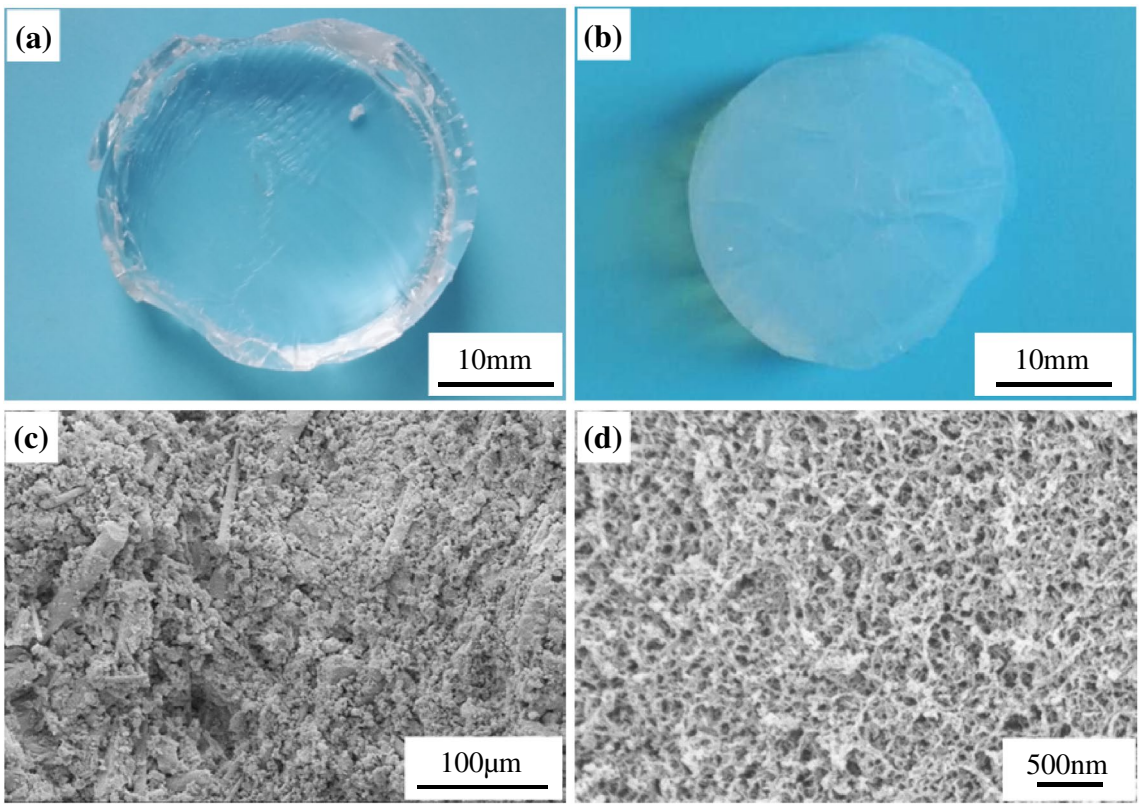

Fig. 2 The macrographs of Al_2O_3–SiO_2 wet gels (**a**) and Al_2O_3–SiO_2 aerogel (**b**); SEM micrographs of Al_2O_3–SiO_2 aerogel/porous zirconia composites (**c**, **d**)

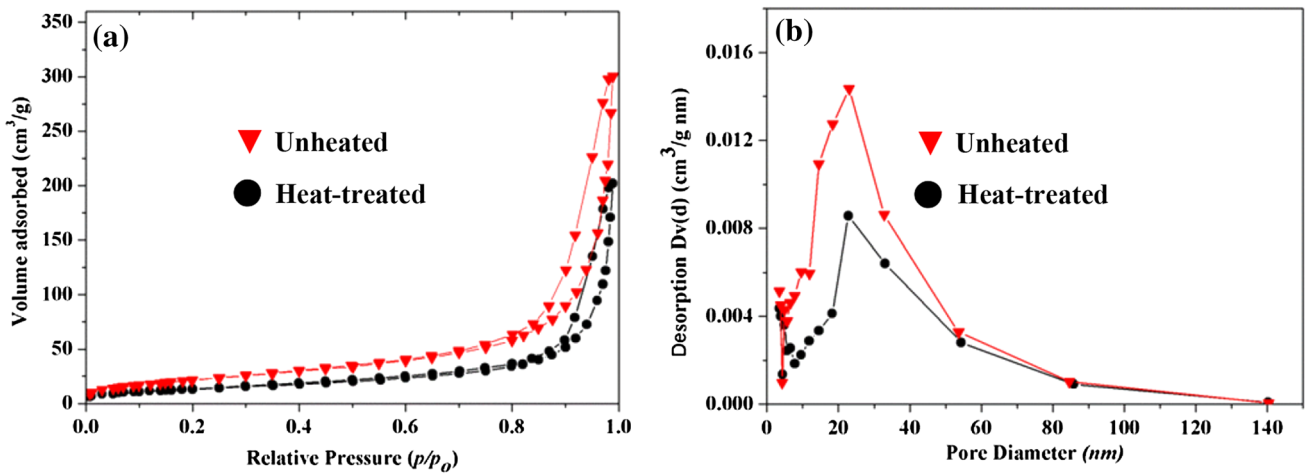

Fig. 3 Nitrogen adsorption–desorption isotherms (**a**) and pore size distribution (**b**) of unheated and heat-treated Al_2O_3–SiO_2 aerogel/porous zirconia composites

region (2–50 nm). The peak pore diameter of unheated composites is about 23 nm, the heat-treated composite (Fig. 3b) shows a broader pore size distribution with a sharp peak at ~25 nm. It indicated that the aerogels of the composites maintained mesopore even after high temperature heat treatment.

Table 2 shows the porosity, density, compressive strength and thermal conductivity of fibrous porous zirconia ceramics before and after impregnation with Al_2O_3–SiO_2 aerogel. After impregnation, the density and compressive strength of the samples increased from 0.53 to 0.59 g/cm^3 and 0.91 to 1.36 MPa, respectively; the porosity and thermal conductivity decreased from 91.3 to 87.1% and 0.066 to 0.049 W/m/K, respectively. As we all know, the strength of porous ceramics is a function of its porosity, so the improvement in strength was mainly attributed to a decreased porosity. The effective total thermal conductivity of porous ceramics can be expressed as follows [25]:

$$\lambda_{total} = \lambda_s + \lambda_g + \lambda_r = \frac{1}{3}\int C_V \rho v_{ph} l_{ph} + \frac{\Pi \cdot \lambda_{g,0}(T)}{1 + \frac{p_{1/2}(T)}{P_g}} + \frac{16 n^2 T_r^3}{3\rho \cdot (T)} \quad (1)$$

where λ_s is the solid thermal conductivity, λ_g is the effective thermal conductivity of the gaseous phase, λ_r is the radiative conductivity; C_v is the specific heat capacity at constant volume, ν_{ph} is the mean velocity of phonons in the material, ρ is the density of the foam, l_{ph} is the phonon mean free path; Π is the porosity of the materials, $\lambda_{g,0}$ is the thermal conductivity of the nonconvecting free gas, $p_{1/2}$ is the gas pressure at which the thermal conductivity is one-half of $\lambda_{g,0}$; n is the effective index of refraction, Tr is the mean radiative temperature, $e(T)$ is the temperature dependent effective specific extinction coefficient. Figure 4 showed the thermal conductivity of fibrous porous zirconia ceramics before and after the impregnation of Al_2O_3–SiO_2 aerogel at elevated temperatures (20–1000 °C), which indicated that the Al_2O_3–SiO_2 aerogel/porous zirconia composite exhibits lower thermal conductivity at the corresponding temperatures. According to Eq. 1, the reasons for the Al_2O_3–SiO_2 aerogel/porous zirconia composite with lower thermal conductivity are as following: firstly, the average pore size of aerogel (<50 nm) is smaller than the mean free paths of oxygen and nitrogen (approximately 70 nm) in air (Fig. 3), which can decrease the effective thermal conductivity of the gaseous phase (λ_g). Secondly, the addition of aerogels considerably enhanced the grain boundary scattering, which obviously decreased the solid thermal conductivity (λ_s). Moreover, as shown in Fig. 4, the thermal conductivity of fibrous porous zirconia ceramics decreased from 0.066 to 0.061 W/(m/K) and then gradually increased to 0.114 W/(m/K). After impregnation, the

Table 2 Porosity, density, compressive strength and thermal conductivity of fibrous porous zirconia ceramics before and after impregnation with Al_2O_3–SiO_2 aerogel

Sample	Density (g/cm^3)	Porosity (%)	Strength (MPa)	Thermal conductivity (W/m/K)
Before impregnation	0.53	91.4	0.86 ± 0.04	0.066 ± 0.003
After impregnation	0.59	87.3	1.22 ± 0.02	0.049 ± 0.002

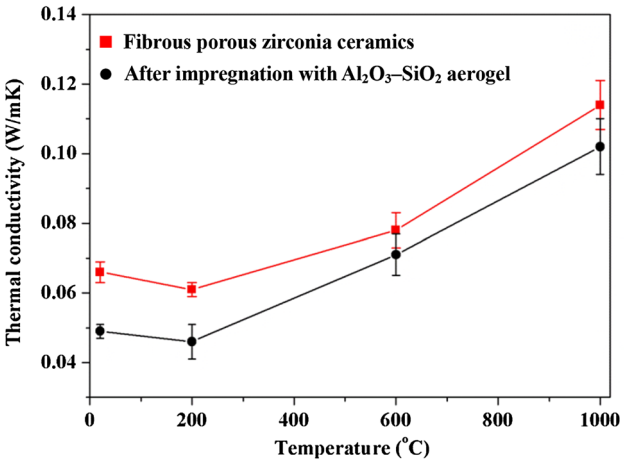

Fig. 4 The thermal conductivity of fibrous porous zirconia ceramics before and after impregnation with Al_2O_3–SiO_2 aerogel at elevated temperatures

thermal conductivity of Al_2O_3–SiO_2 aerogel/porous zirconia composite decreased from 0.049 to 0.046 W/(m/K) and then gradually increased to 0.102 W/(m/K). As far as we know, the effective total thermal conductivity of porous ceramics is mainly dependent on the the solid thermal conductivity (λ_s) at low temperatures. The reason that the solid thermal conductivity (λ_s) of porous ceramics at 200 °C is much lower than that of the samples at room temperature is because the phonon means free paths (l_{ph}) of inorganic materials usually decrease with increasing temperature from room temperature to Debye temperature [26]. As the temperature is further increased, the radiative conductivity (λ_r) becomes dominant, it can be attributed to the fact that it is proportional to T^3. Meanwhile, the solid thermal conductivity (λ_s) of the porous ceramics is nearly constant because the phonon means free paths (l_{ph}) are approximately temperature-independent above the Debye temperature. Therefore, as showed in Fig. 4, the total thermal conductivity of both fibrous porous zirconia ceramics and Al_2O_3–SiO_2 aerogel/porous zirconia composite showed a linear increase above 400 °C.

4 Conclusions

Highly fibrous porous zirconia ceramics with low thermal conductivity and high strength were prepared by vacuum squeeze moulding. As the B_4C content was increased from 0 to 1 wt%, the thermal conductivity of fibrous porous zirconia ceramics decreased from 0.064 to 0.060 W/m/K, and the compressive strength increased from 0.22 to 0.44 MPa. As the B_4C content further increased to 4 wt%, the thermal conductivity increased to 0.076 W/m/K, and the compressive strength of the samples decreased to 0.31 MPa. As the SiC content was increased from 10 to 20 wt%, the compressive strength and thermal conductivity of fibrous porous zirconia ceramics in the z-direction increased from 0.44 to 0.91 MPa and 0.060 to 0.076 W/(m/K), respectively. After impregnating fibrous porous zirconia ceramics with Al_2O_3–SiO_2 aerogels, the compressive strength of the samples increased from 0.86 to 1.22 MPa, and the thermal conductivity decreased from 0.066 to 0.049 W/m/K in the z direction. Moreover, the Al_2O_3–SiO_2 aerogel/porous zirconia composite also exhibits better thermal insulating properties at high temperatures.

Acknowledgements This work was supported by the National Natural Science Foundation of China (11672031 and 11472038), the Fundamental Research Fund for the Central Universities (Grant No. 2014RC047) and China Scholarship Council.

References

1. B. Nait-Ali, K. Haberko, H. Vesteghem, J. Absi, S. D., Smith. J. Eur. Ceram. Soc. **26**, 3567 (2006)
2. X.H. Zhang, R.B. Zhang, G.Q. Chen, W.B. Han, Mater. Sci. Eng. A **497**, 195 (2008)
3. P.Q. Yuan, Y. Liu, F. Bai, L. Xu, Z.M. Cheng, W.K. Yuan, Catal. Commun. **12**, 753 (2011)
4. J. Tan, Y.C. Su, T. Hu, Q.S. Yu, R. Tursun, Q. Li, Y.Z. Xi, Solid State Ion. **292**, 22 (2016)
5. D.Y. Li, M.S. Li, J. Porous Mater. **19**, 345 (2012)
6. A. Kumar, K. Mohanta, D. Kumar, O. Parkash, Microporous Mesoporous Mater. **213**, 48 (2015)
7. B.Y. Han, R.B. Zhang, D.N. Fang, J. Porous Mater. **23**, 563 (2016)
8. K.W. Schlichting, N.P. Padture, P.G. Klemens, J. Mater. Sci. **36**, 3003 (2001)
9. L.F. Hu, C.A. Wang, Y. Huang, J. Mater. Sci. **45**, 3242 (2010)
10. J.C. Han, C.Q. Hong, X.H. Zhang, J.C. Du, W. Zhang, J. Eur. Ceram. Soc. **30**, 53 (2010)
11. Y.H. Dong, C.A. Wang, J. Zhou, Z.L. Hong, J. Eur. Ceram. Soc. **32**, 2213 (2012)
12. X.H. Ma, X.X. Hu, H.Y. Du, H.Y. Lv, J. Eur. Ceram. Soc. **36**, 797 (2016)
13. J.J. Sun, Z.J. Hu, J.N. Li, H.B. Zhang, C.C. Sun, Ceram. Int. 40, 11787 (2014)
14. R.B. Zhang, X.B. Hou, C.S. Ye, B.L. Wang, D.N. Fang, J. Eur. Ceram. Soc. **36**, 3539 (2016)
15. R.B. Zhang, C.S. Ye, X.B. Hou, S.H Li, B.L. Wang, Ceram. Int. **42**, 14843 (2016)
16. J. Fricke, M.C. Arduini, D. Buttner, H.P. Ebert, U. Heinemann, Therm. Conduct. **77**, 235 (1990)
17. R.B. Zhang, Q. Qu, B.Y. Han, B.L. Wang, Mater. Lett. **175**, 219 (2016)
18. L. Xu, Y.G. Jiang, J.Z. Feng, J. Feng, C.W. Yue, Ceram. Int. **41**, 437 (2015)
19. J. He, X.L. Li, D. Su, H.M. Ji, X.J. Wang, J. Eur. Ceram. Soc. **36**, 1487 (2016)
20. S.N. Karlsdottirw, J.W. Halloran, A.N. Grundy, J. Am. Ceram. Soc. **91**, 272 (2008)
21. W.D. Kingery, H.K. Bowen, D.R. Uhlmann, *Introduction to Ceramics*, 2nd edn. (Wiley, New York, 1976)
22. T.F. Baumann, A.E. Gash, S.C. Chinn, A.M. Sawvel, J.H.S. R.S. Maxwell, Jr, Chem. Mater. **17**, 395 (2005)

23. S. Brunauer, L.S. Deming, W.E. Deming, E. Teller, J. Am. Chem. Soc. **62**, 1723 (1940)
24. Y.T. Bi, H.B. Ren, B.W. Chen, G. Chen, Y. Mei, L. Zhang, J. Sol–Gel Sci. Technol. **63**, 140 (2012)
25. H.P. Ebert, Thermal Properties of Aerogel, in *Aerogels Handbook*, ed. by A.A. Aegerter, A. Leventis, M.M. Koebel (Springer, New York, 2011), pp. 537–564
26. H.R. Lu, C.A. Wang, Y. Huang, H.M. Xie, Sci. Rep. **4**, 6823 (2014)